Benchmarking Resilience and Sensitivity of Polyurethane-Based Vision-Based Tactile Sensors

Benjamin Davis and Hannah Stuart*

Abstract— Vision-based tactile sensors (VBTSs) are a promising technology for robots, providing them with dense signals that can be translated into an understanding of normal and shear load, contact region, texture classification, and more. However, existing VBTS tactile surfaces make use of silicone gels, which provide high sensitivity but easily deteriorate from loading and surface wear. We propose that polyurethane rubber, used for high-load applications like shoe soles, rubber wheels, and industrial gaskets, may provide improved physical gel resilience, potentially at the cost of sensitivity. To compare the resilience and sensitivity of silicone and polyurethane VBTS gels, we propose a series of standard evaluation benchmarking protocols. Our resilience tests assess sensor durability across normal loading, shear loading, and abrasion. For sensitivity, we introduce model-free assessments of force and spatial sensitivity to directly measure the physical capabilities of each gel without effects introduced from data and model quality. Finally, we include a bottle cap loosening and tightening demonstration as an example where polyurethane gels provide an advantage over their silicone counterparts.

I. INTRODUCTION

The importance of tactile sensing in robotics is becoming increasingly recognized as robots transition from controlled laboratory environments to more structured and unpredictable scenarios like homes, factories, or elsewhere. Tactile sensing, the robotic equivalent of the human sense of touch, provides information about physical interactions with objects and the environment that allows robots to perform complex manipulation tasks, handle delicate objects, adapt to their surroundings, and recover from mistakes. Extensive research has been performed on the development and improvement of a range of tactile sensing technologies, including capacitive/piezoresistive/piezoelectric sensors, barometric sensors, and vision-based (or optical) tactile sensors [1], [2].

A. Vision Based Tactile Sensors

Among these technologies, vision-based tactile sensors (VBTSs) are increasingly promising due to the rich information they provide (e.g., Digit [3], Gelsight [4]). These sensors operate by using an internal camera to observe the deformation of a soft elastomer that physically contacts the environment. The gel's deformation is captured by an image transfer layer–often reflective and/or covered with a pattern of markers–which is cast onto a transparent base layer. This assembly is then adhered to an acrylic window in front of the internal camera [5]. In existing work, both layers are

Benjamin Davis and Hannah Stuart are with the Embodied Dexterity Group, Dept. of Mechanical Engineering, University of California Berkeley, Berkeley, CA, USA.
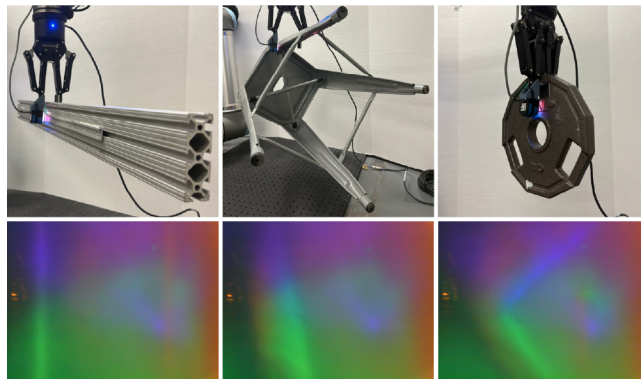
*Corresponding author: hstuart@berkeley.edu

Fig. 1. Our polyurethane VBTS gel is capable of performing grasps without failure on rugged, heavy objects, including a 23.5 N piece of aluminum extrusion (left), a 40 N stool (center), and a 44.5 N weight (right).

typically made with silicone, a soft elastomer that provides high sensitivity during contact. VBTSs offer multiple advantages over more traditional tactile sensors, including high-resolution data, reduction of custom wires and circuitry, and the removal of electronics from the tactile interface itself [5]. The visual data from the sensor can be processed to extract many types of information, such as contact region, normal and shear forces, texture classification, pose estimation, and slip detection [6], [7], [8], [9], [10], [11].

B. Durability

However, one major limitation of VBTSs is the durability of their silicone gels. These gels have multiple known failure modes, including surface wear of the image transfer layer via abrasion/scratching/tearing and delamination of the silicone from the acrylic window [12], [13], [14]. While their performance may be suitable for in-lab data collections and demonstrations, their deployment in the real world requires sensors that can endure repeated and unexpected use. Prior work has sought to improve the durability of gels by covering the sensor with a protective material, such as latex or tape [15], [16], [13], [14]. However, these protective layers can cause artifacts in the image [13], [14] and often need replacing. Different works have also experimented with silicones of varying hardness [5]. The low bond strength of silicone to acrylic, which leads to delamination failures, remains a problem across these approaches. As a result, most existing VBTS applications are currently limited to low-force manipulation tasks. In practice, these sensors may endure higher loads–possibly unexpectedly–and require an increased

level of sensor resilience to various forms of loading and abrasion.

To address the need for a more resilient VBTS in home or industrial settings, we propose a new polyurethane-based gel. Polyurethane is used in various high-wear applications like shoe soles, skateboard wheels, and industrial gaskets, and may provide a significant lifespan improvement over its silicone counterparts. Polyurethane also bonds well to acrylic via superglue, which would reduce delamination failures. We predict that polyurethane will provide a more resilient alternative to silicone for VBTSs, although we expect that this will come at the cost of sensitivity.

C. Benchmarking methods

Limited work has formally assessed the durability of VBTS gels, and existing assessments focus only on a single, specific mode of failure [3], [15], [12]. In reality, sensor gels will experience wear from a combination of different types of loading and rubbing. Additionally, while recent years have yielded many evaluations of VBTS performance [17], [18], [19], these evaluations are all model-based. As a result, their performance metrics depend on the specific model and dataset, which can obscure a direct understanding of the sensor's intrinsic physical capabilities. While these model-based evaluations are useful for assessing performance in specific application contexts, we argue that a complementary, model-free evaluation can enable quicker, simpler baseline comparisons of sensitivity across different hardware platforms.

To address these two concerns, we propose a collection of mechanical tests to evaluate sensitivity across a potential lifetime of wear, including compressive loading, shear loading, and abrasion. We also introduce model-free evaluations of sensitivity–specifically, force and spatial sensitivity–to allow for baseline comparisons across silicone and polyurethane VBTS gels. Our proposed spatial sensitivity evaluation uses frequency domain analysis to extract signal strength from a ridged surface with known period and amplitude. We take inspiration from grating orientation discrimination tasks, which have been used to assess tactile spatial sensitivity in humans [20], [21], [22]. This task involves pressing a ridged surface onto a subject's finger and examining whether they can correctly report its vertical or horizontal orientation. Recent work emulates this test, relying on the Structural Similarity Index Measure (SSIM) and a support vector machine (SVM) classifier to determine a tactile sensor's ability to distinguish between vertical or horizontal ridges [17]. However, this approach still relies on data collection and model training, and the use of SSIM (which reflects human visual perception) may present biases compared to the use of raw sensor data.

D. Overview

We present three novel contributions in this work:

1) The development of a polyurethane-based VBTS gel
2) VBTS mechanical resilience evaluations
3) VBTS model-free sensitivity evaluations

We begin by describing both our silicone and polyurethane gel fabrication techniques in Section II. Then, we present the parameters and procedures for our resilience and sensitivity evaluations in Section III. The results of these tests demonstrate that the polyurethane gel is more physically robust than the silicone gel, in Section IV, and outcomes are discussed in V. Finally, we include a repetitive bottle cap loosening and tightening demonstration in Section VI before concluding in Section VII.

II. GEL FABRICATION

In this section, we describe our fabrication techniques for producing the silicone and polyurethane gels used for comparison. We use the body of the DIGIT [3] as a base, which contains a camera and three RGB LEDs. It uses a gel composed of a transparent silicone base layer (Smooth-On Solaris, Shore A 15) and an opaque image transfer layer (Smooth-On EcoFlex 00-10, Shore 00-10) colored with white pigment and airbrushed onto the base layer. This gel is glued onto an acrylic window with Smooth-On Sil-Poxy. The acrylic-gel unit can then be press-fit into the DIGIT case. Due to the DIGIT's modularity and open-sourced design, we are able to develop and test custom acrylic-gel units with silicone and polyurethane. We choose to make our gels flat rather than rounded like the original DIGIT gels for ease of fabrication and better compatibility with our tests. We describe our manufacturing processes for each material below.

1) Silicone Gels: We first create the silicone base layer with equal parts A and B (by weight) of Smooth-On Solaris. The mixture is degassed and then poured into a 4mm deep 3D printed mold to cure. To form the image transfer layer, we combine equal parts A and B of EcoFlex 00-10. We then mix in 10% by weight of Smooth-On Silicone Thinner, which reduces layer thickness for improved sensitivity, and 1% by weight of Smooth-On Cast Magic Silver Bullet powder and 2% by weight of Smooth-On Silc Pig white pigment, both of which contribute to lower opacity and higher reflectivity. To combine the base layer and image transfer layer, we place the cured base layer facing upwards on a flat acrylic plate, and the uncured image transfer layer mixture is poured over until it is covered. We found that this method produces an image transfer layer thicker than that of the original DIGIT, and thus less sensitive. To counter this, we use an air blow gun to gently displace some of the uncured material off the top of the base layer. While a more standardized procedure like spin-coating would provide better consistency, we find that our method is sufficient for small batches. After this step, we leave the silicone to cure for four hours. Once completely cured, we use a razor blade to clean up the edges of the gel before gluing it to a 6.35mm thick clear acrylic window with Smooth-On Sil-Poxy.

2) Polyurethane Gels: To form the base layer of the polyurethane gel, we use equal parts by weight of Smooth-On Clear Flex 50 (Shore A 50) Parts A and B. We mix thoroughly and degas before pouring into a silicone negative mold created with a 3D printed positive and letting cure. The
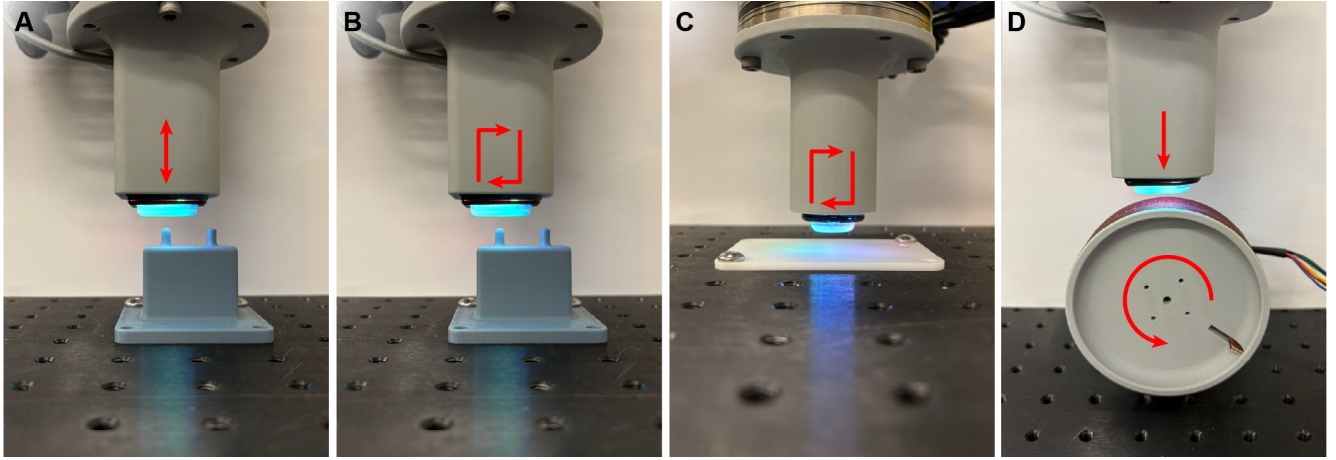
Fig. 2. We perform four resilience tests: (A) cyclic compression on an indenter, (B) cyclic local shear on an indenter, (C) cyclic transverse shear on a flat surface, and (D) abrasion. The setup in (A) is also used to characterize the sensor's force sensitivity.

image transfer layer is created by mixing equal parts A and B of Smooth-On VytaFlex 40. To this mixture, we add 1% by weight of Smooth-On Cast Magic Silver Bullet powder and 2% by weight of Smooth-On SO-Strong white urethane colorant and mix thoroughly. To attach the base and image transfer layers, we first pour 0.25 g of the uncured image transfer layer mixture into the base of the emptied silicone mold. The specific volume of VytaFlex 40 is 971.8 $\frac{\text{mm}^3}{\text{g}}$, yielding a layer height of approximately 0.62 mm (not considering mix-ins or mold fillets). We then use an air blow gun to gently spread the mixture along the base of the mold and remove large bubbles by popping with tweezers. Next, we place the base layer back into the mold and press it down onto the uncured image transfer layer, ensuring that no air is captured in pockets between the layers. Once placed evenly, the gel is left to cure. The cured gel is then attached to an acrylic window by spreading superglue across the surface of a window, pressing the gel on firmly, and wiping away excess glue.

III. SENSOR BENCHMARK METHODS

A. Mechanical Resilience Characterization

To characterize the mechanical resilience of our silicone and polyurethane gels, we put them through a series of mechanical tests that target different forms of loading or wear that may be encountered during use. As shown in Fig. 2, We include three categories of testing: compression, shear, and abrasion. We perform all tests with the sensor mounted to a Universal Robots UR-10 robot arm.

1) Cyclic Compression Loading: We first test the gel's ability to withstand stretching or puncture from repeated compressive loading with the setup in Fig. 2A. Compressive loads may occur often during the lifetime of the sensor as it is used to grasp objects. We perform this test on a 4 mm spherical tip indenter with a 15 N compressive load and 1000 cycles. We selected a 15 N load through experimentation, increasing the load until failure was observed for

either material. This loading is on the high end of typical human grasp forces [23] but could easily be surpassed in more industrial settings [24]. We test for 1000 cycles to approximate a lifetime of sensor use.

2) Cyclic Shear Loading: We also test the gel's resilience under shear. We include both local shear and transverse shear, or shear across the whole face of the sensor. For local shear, we compress the sensor onto a 4 mm spherical tip indenter with a 10 N compressive load, and then apply a 5 N lateral load. This setup is shown in Fig. 2B. We choose a 10 N compressive load as it does not induce failure in either material alone within 1000 cycles, as revealed during the force selection process for the cyclic compression test. These loadings are similar to what humans might experience lifting a 500 g object with a small point of contact, assuming a static friction coefficient of ∼0.5. For transverse shear, we compress the sensor onto a flat acrylic plate with a 15 N compressive load and then apply a 15 N lateral load, as seen in Fig. 2C. We apply a 15 N compressive load to increase friction forces and prevent the gel from slipping on the plate. We include this test primarily to target delamination failures. The tests for local shear and shear across the whole gel are both run for 1000 cycles.

3) Abrasion: To test the gel's abrasion resistance, we abrade it with a custom setup shown in Fig. 2D. We wrap 150 grit sandpaper around a 3D printed 95.5 mm diameter wheel controlled with a brushed DC motor. The robot arm presses the gel against the sandpaper with 5 N of force. We then spin the wheel against the gel at constant velocity for 8 m in 2 m increments, where an unloaded sensor image is captured after each increment. The sandpaper is replaced before every full 8 m trial and used for its entire duration.

4) Evaluation: We evaluate all resilience tests with the same metric. For each cycle, we record 10 RGB frames of both the unloaded and loaded sensor readings at 30 frames per second with QVGA resolution (320x240 pixels) and average them to get one unloaded and one loaded image per cycle. For abrasion, we only record unloaded frames.
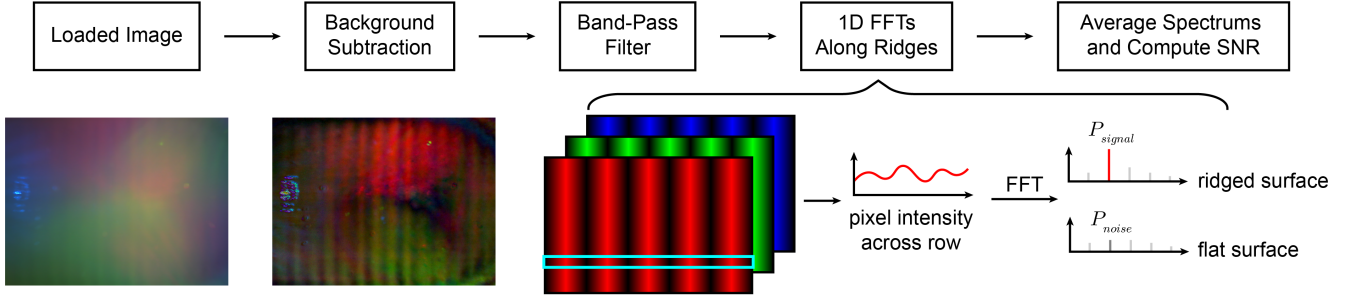
Fig. 3. Our model-free spatial sensitivity evaluation uses the sensor reading when pressed onto a ridged surface. The image is preprocessed via background subtraction and bandpass filtering before being cropped and run through a series of 1D FFTs. The resulting power spectral densities are averaged. The signal power is compared to a noise power, defined by the same frequency range from a flat, ridgeless surface, to obtain a signal-to-noise ratio (SNR). The background subtraction image is amplified for visualization purposes.

To evaluate sensor damage, we calculate the mean absolute error (*MAE*) between the image at the current cycle and the image at the first cycle separately for unloaded and loaded images:

$$MAE_n = \frac{1}{320 \times 240 \times 3} \sum_{i=1}^{320} \sum_{j=1}^{240} \sum_{c=1}^{3} |I_n(i,j,c) - I_1(i,j,c)| \quad (1)$$

where n represents the current cycle, i and j are the pixel coordinates, c is the color channel (RGB), and I_n and I_1 are the images of the current cycle and first cycle, respectively. This metric directly measures how much the sensor reading changes due to wear.

B. Sensitivity

Improving sensor resilience typically reduces sensitivity. To capture these downsides, we propose two tests to evaluate force sensitivity and spatial sensitivity.

1) Force Sensitivity: We evaluate the force sensitivity of our different sensor gels, without durability testing, by loading them up to 40 N on a 4 mm spherical tip indenter at a rate of $2e^{-6}$ m/s. We use the same setup used for cyclic compression (Fig. 2A). We restrict the maximum load to 40 N due to hardware limitations, although this range is sufficient for distinguishing silicone and polyurethane performance. During a single loading and unloading, we record 320x240 RGB frames at 30 frames per second with the DIGIT sensor and normal forces with a force torque sensor (ATI Axia80-M8). We then calculate the *MAE* of each frame with respect to the first frame to quantify how much the captured image changes with loading.

2) Spatial Sensitivity: Our approach for assessing spatial sensitivity in vision-based tactile sensors is a novel, model-free method that analyzes features directly rather than relying on model training. We accomplish this by performing a frequency-domain analysis of the sensor's measurement of a periodic, ridged surface. By varying the period of the ridges, we can assess x/y sensitivity; similarly, we can evaluate z-sensitivity by varying amplitude. The process is depicted in Fig. 3.

First, the sensor is pressed against the ridged surface with a known period and amplitude. We record 500 frames of RGB image data at 30 frames per second at a resolution of 640x480 pixels. We record another 500 frames with the sensor unloaded. The sequences of 500 frames are averaged to mitigate the effects of random noise, yielding one unloaded image and one loaded image.

We then preprocess the images to clean the signal. First, we perform background subtraction between the unloaded and loaded frames, $I_{delta} = I_{loaded} - I_{unloaded}$, to isolate the changes observed due to sensor gel deformation. Next, the image is spatially filtered to remove low-frequency artifacts and high-frequency noise using a difference of Gaussians method. Finally, the image is cropped to limit effects caused by camera distortion and the edges of the gel.

To quantify the sensor's spatial response, we perform a series of one-dimensional Fast Fourier Transforms across each row of pixels spanning the ridged pattern for each color channel, centering to eliminate the DC component. We then calculate power spectrums and average across all rows and channels to obtain a single non-normalized power spectral density (PSD) for the sensor's signal. We use this spectrum to calculate spatial sensitivity using a Signal-to-Noise Ratio (SNR). The noise floor is obtained by recording the PSD on a flat, ridgeless surface. Next, we calculate signal power P_{signal} for a ridged surface as the summed power of the two frequency bins closest to the the known ridge frequency. We define the noise power P_{noise} as the summed power of the corresponding frequency bins from the spectrum of the flat surface (Fig. 3). Finally, we calculate SNR in decibels (dB) as follows:

$$SNR_{dB} = 10 log_{10} \left(\frac{P_{signal}}{P_{noise}} \right). \quad (2)$$

In this study, we test across 10 ridge amplitudes with constant period, and 10 ridge periods with constant amplitude. All ridges were printed with custom settings on a Bambu X1E. We test across amplitudes of 0.005 to 0.05 mm, and across periods of 0.6 mm to 1.5 mm. Ridges of varying magnitude all have the maximum period of 1.5 mm, while ridges of varying period have the same maximum amplitude of 0.6 mm. We selected these ranges experimentally to to capture interesting results, ensuring that both materials could generate a meaningful signal at the largest period and

amplitude. We also test each ridge with a 2 N and 10 N normal load to observe how it affects spatial sensitivity.

IV. RESULTS

A. Mechanical Resilience

Resilience testing results are presented in Fig. 4. Due to variations in the sensor gel that can occur during the manufacturing process, we perform our mechanical resilience tests on three different gels for each material, resulting in six total trials per test. Different gels are used for each test, thus 24 gels were fabricated in total for these particular results. For visualization of relative silicone and polyurethane gel wear, we include representative unloaded sensor images after the test concluded from the first of the three gel samples of each material.

1) Cyclic Compression Loading: Results from the cyclic compressive loading test can be found in Fig. 4A. Silicone samples 1 and 2 fail catastrophically due to puncture within 250-500 cycles, leading to large increases in *MAE*. The third sample undergoes a much smaller increase in MAE throughout the test. This gel's image transfer layer undergoes permanent visible deformation from the indenter, but puncture does not occur. All three polyurethane gels see minimal change in the unloaded and loaded images throughout the test, consistently outperforming the silicone gels.

2) Cyclic Shear Loading: Fig. 4B shows the results of cyclic local shear loading with an indenter for the different gel materials. Silicone samples 1 and 2 encounter catastrophic failure with puncture and tearing occurring before 500 cycles of loading. The third sample undergoes a less noticeable over the course of the test. Puncture still occurs for this gel, but the hole is clean and only induces a small increase in *MAE* relative to the other two silicone samples. Again, the polyurethane gels consistently outperform the silicone gels, seeing minimal changes in reading throughout the test.

For transverse shear on a flat surface, results in Fig. 4C show limited change in reading across the 1000 cycles. The silicone gels undergo varying degrees of minor delamination from the acrylic window, with the first sample seeing the largest amount. Still, the *MAE* is limited to ∼7 units per pixel when unloaded and ∼5 when loaded for this gel, which is much less than that observed for cyclic compression and shear failures on the indenter. The polyurethane gels provide relatively constant images throughout the cycles, with no visible delamination present.

3) Abrasion: Abrasion testing results are shown in Fig. 4D. The three silicone gels experience varying degrees of tearing in the image transfer layer, often occurring within 2 m of abrasion and increasing with more distance. The polyurethane gels also experience noticeable wear during the test, although a limited increase in *MAE* indicates that the sensor reading does not experience much change. During testing, the polyurethane image transfer layer was observed to wear away as small particles rather than tear from the clear base layer in bulk like their silicone counterparts, leading to this improvement in performance.

B. Sensitivity

1) Force Sensitivity: Results in Fig. 5A show that silicone gels provide much higher force sensitivity for loads less than 10 N. However, once the load increases beyond this point, the signal from the silicone begins to saturate. Conversely, the polyurethane gel provides a lower but more consistent sensitivity across the entire loading range, indicating its usefulness for higher load applications.

2) Spatial Sensitivity: The results from our spatial sensitivity test, shown in Fig. 5B, illustrate the performance of both materials across the different ridged surfaces and loading conditions. With a 2 N load, the silicone gels generally perform as well as or better than their polyurethane counterparts. For constant period tests, both gels demonstrate a gradual increase in performance with increasing amplitude, with SNR plateauing at 10-15 dB for amplitudes larger than 0.03 mm. For constant amplitude tests, silicone gels provide much clearer signals, especially for periods of 1.0 mm or smaller. When the load is increased to 10 N, the SNR increases for polyurethane but reduces for silicone, resulting in better relative performance for polyurethane across most ridges. The reduction of silicone gel performance at higher load can be attributed to an increase in noise power and may not reflect a decrease in the sensor's ability to detect the ridges. We discuss this further in Section V. Both sensors show the same general trends across surfaces, seeing plateaus in performance once the ridges reach an amplitude of 0.035 mm or a period of 1.1 mm.

V. DISCUSSION

Our results show that polyurethane-based vision-based tactile sensor gels can outlast silicone-based gels across multiple types of wear, including local compression and shear, transverse shear across the whole gel, and abrasion. Additionally, the polyurethane gels may provide improved sensitivity for large forces, where silicone gels may saturate or become noisy due to large deformations. We propose that each sensor has its use case. At low forces, we find that silicone provides improved force and spatial sensitivity, making it an ideal choice for tasks requiring higher precision. However, if sensor reliability or operation at high forces are necessary, our results suggest that polyurethane gels offer an advantage.

We note that our evaluation techniques face certain limitations. The *MAE* used in our resilience tests shows how much the sensor reading has changed without characterizing how this change affects sensor performance. It is possible that performance can be recovered through sensor recalibration or better models, but we leave this to future work. Our resilience tests–while designed to be representative of real wear–are also highly controlled, with set contact geometries and loading forces. Thus, we do not expect the test lifetimes of our sensors to directly represent their cyclic lifetime in application, and we primarily emphasize the relative performance of each material in these tests.

Although not validated in this work, we hypothesize that our spatial sensitivity results correspond with each gel's
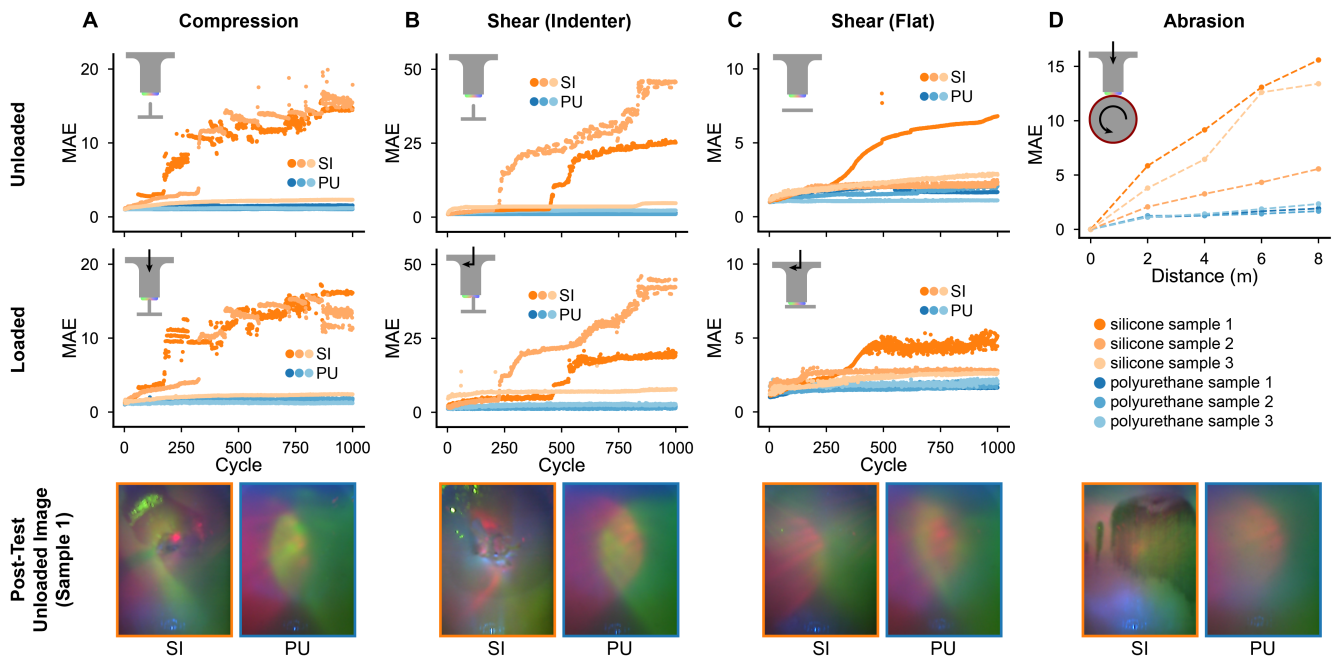
Fig. 4. Results for cyclic compression (A), cyclic shear on an indenter (B), cyclic shear on a flat surface (C), and abrasion (D) tests across three gel samples for silicone (SI) and polyurethane (PU). The first row represents sensor images captured at each cycle after unloading, while the second row shows results from loaded images. The raw sensor images in the third row depict the final unloaded sensor image (after 1000 cycles) from sample 1 of each material. Different sets of gels are used for each test.
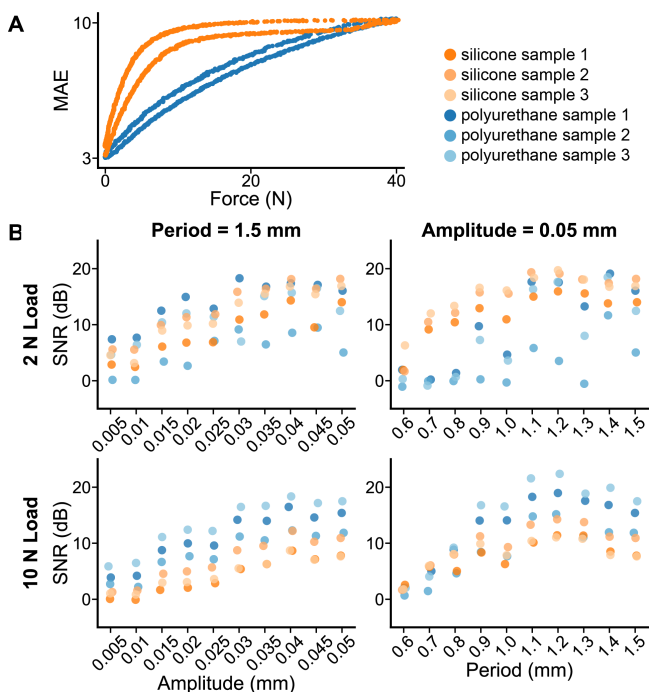

Fig. 5. Results for force sensitivity (A) and spatial sensitivity (B) tests. In (A), the mean absolute error (MAE) is calculated with respect to the unloaded image to quantify signal change across force. In (B), the first and second rows show SNR under 2 N and 10 N loads, respectively. The left and right columns represent tests with varying amplitude (constant period) and period (constant amplitude).

minimum detectable geometries, i.e. that a gel's signal strength for a ridge of certain amplitude and period reflects its ability to detect features of similar size. The strength of this relationship should be explored in future work. However, sensor performance in our evaluation depends also on loading force. Increasing the loading force can improve signal power, leading to improved SNR as seen with the polyurethane gels. But, larger forces also increase the bulk deformation of the sensor, generating large changes in the sensor image that remain after background subtraction. When the sensor is loaded onto a flat surface to define the noise floor, these changes can increase noise power across frequency bins, leading to reduced SNR for the silicone gels. In application, inference models can be trained on high loads directly and would likely not suffer the same performance drop. We acknowledge this as a limitation of our model-free evaluation, and future work should investigate different pre-processing techniques and noise floor definitions to reduce this effect.

In this work, we only compare between one type of polyurethane gel and one type of silicone gel. Different polyurethanes, silicones, and fabrication techniques may result in changes to relative performance and should be explored in future work.

VI. DEMONSTRATION

To demonstrate the resilience and performance of both sensors in application, we perform a repeated task of loosening and tightening a bottle cap (Fig. 6B), which induces both compressive and shear loads as well as local surface wear. We use a Robotiq 2F-140 parallel jaw gripper attached to a
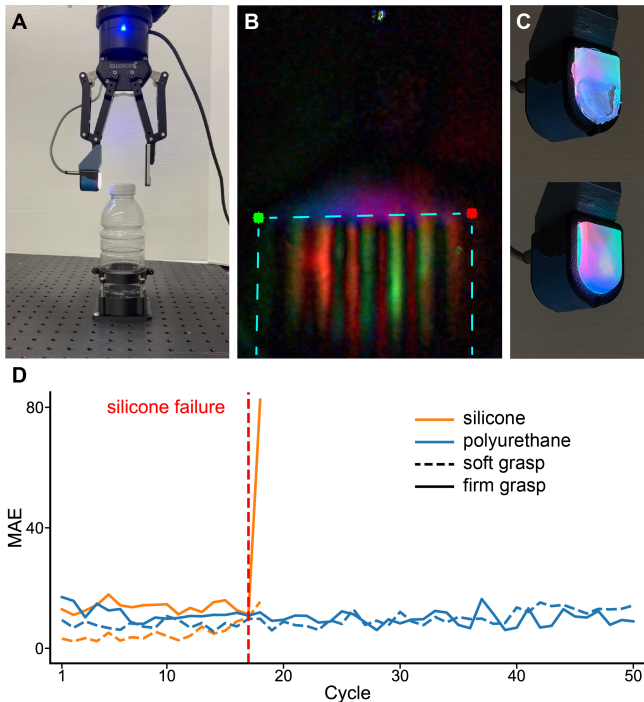
Fig. 6. For demonstration, we perform repeated loosening and tightening of a bottle cap with a sensorized gripper (B). A trained CNN predicts two points that define a simplified contact region shown with dashed lines (C). Mean absolute errors (MAE) of model predictions are calculated for the soft and firm grasps performed during tightening at each cycle (A). The silicone gel tears after 16 cycles (D, top) and is unable to carry on, while the polyurethane gel remains undamaged (D, bottom).

UR-10 robot arm. For each material, we train a convolutional neural networks (3 convolution layers, 1 hidden dense layer) to predict two points defining a simplified contact region (Fig. 6C). Training data includes background-subtracted images with hand annotations from 243 grasps of varying force and location, augmented by random translations with a custom data generator during training.

We then conduct (up to) fifty cycles of the task, first loosening and then re-tightening a ridged bottle cap to a max torque of 0.8 N-m. During the re-tightening phase, the robot performs a small initial rotation with a soft grasp, resets, and then grasps firmly to tighten the remainder of the way, resulting in two grasps per cycle. The grasp force of the Robotiq 2F-140 is not directly controllable, so the force parameters are set experimentally to ensure a secure grasp. The sensor images from both re-tightening grasps (before any torque is applied) are annotated by hand, and then predictions are made with the trained models. The mean absolute error of the model predicted contact region at each cycle is shown for both grasps (soft and firm) and both materials 6A.

The silicone gel fails via tearing (6) after the 16th cycle of tightening, resulting in increased prediction errors for both grasps in the 17th cycle. After failure, the gel does not provide enough friction to twist the cap, resulting in an early stoppage. The polyurethane gel successfully completes all 50 cycles, maintaining consistent performance without

visible failure. This demonstration shows an example of a real-life task where polyurethane VBTS gels can provide improved resilience over silicone gels while still providing useful tactile signals.

VII. CONCLUSION

The practical deployment of vision-based tactile sensors in real-world environments is often hindered by a lack of physical sensor resilience, as their silicone gels are prone to tearing, abrasion, and delamination. In this work, we introduce a polyurethane-based gel as a resilient alternative and propose a set of standardized, model-free evaluations to compare its resilience and sensitivity to its silicone counterparts.

The results of our resilience evaluations show that polyurethane gels can indeed outlast silicone gels across repeated cycles of compression, shear, and abrasion, resisting the catastrophic punctures and tears experienced by many of the silicone samples. While our model-free sensitivity analysis confirms that silicone provides enhanced force and spatial sensitivity compared to polyurethane at low load, it also reveals that polyurethane can provide high spatial sensitivity and better force sensitivity with increased load.

The use of silicone or polyurethane gels should depend on the application. For delicate manipulation tasks where high sensitivity to forces and contact geometries are the priority, silicone remains a suitable option. However, for applications where sensors must be deployed into different unstructured environments without easy access to replacements, we suggest that polyurethane gels offer an advantage. But, we test on one specific version of each material, and many silicones and polyurethanes exist with different mechanical properties. Further exploration of materials and fabrication techniques may yield better solutions, and we propose that our resilience and sensitivity evaluation techniques provide simple, consistent ways to compare across them.

ACKNOWLEDGMENT

REFERENCES

[1] Z. Kappassov, J.-A. Corrales, and V. Perdereau, "Tactile sensing in dexterous robot hands — Review," *Robotics and Autonomous Systems*, vol. 74, pp. 195–220, Dec. 2015.
[2] M. R. Cutkosky and W. Provancher, *Force and Tactile Sensing*, pp. 717–736. Cham: Springer International Publishing, 2016.

[3] M. Lambeta, P.-W. Chou, S. Tian, B. Yang, B. Maloon, V. R. Most, D. Stroud, R. Santos, A. Byagowi, G. Kammerer, D. Jayaraman, and R. Calandra, "DIGIT: A Novel Design for a Low-Cost Compact High-Resolution Tactile Sensor with Application to In-Hand Manipulation," *IEEE Robotics and Automation Letters*, vol. 5, pp. 3838–3845, July 2020. arXiv:2005.14679 [cs].

[4] W. Yuan, S. Dong, and E. H. Adelson, "GelSight: High-Resolution Robot Tactile Sensors for Estimating Geometry and Force," *Sensors*, vol. 17, p. 2762, Dec. 2017. Publisher: Multidisciplinary Digital Publishing Institute.

[5] S. Zhang, Z. Chen, Y. Gao, W. Wan, J. Shan, H. Xue, F. Sun, Y. Yang, and B. Fang, "Hardware Technology of Vision-Based Tactile Sensor: A Review," *IEEE Sensors Journal*, vol. 22, pp. 21410–21427, Nov. 2022. Conference Name: IEEE Sensors Journal.

[6] G. Zhang, Y. Du, H. Yu, and M. Y. Wang, "DelTact: A Vision-Based Tactile Sensor Using a Dense Color Pattern," *IEEE Robotics and Automation Letters*, vol. 7, pp. 10778–10785, Oct. 2022.

[7] F. Baghaei Naeini, A. M. AlAli, R. Al-Husari, A. Rigi, M. K. Al-Sharman, D. Makris, and Y. Zweiri, "A Novel Dynamic-Vision-Based Approach for Tactile Sensing Applications," *IEEE Transactions on Instrumentation and Measurement*, vol. 69, pp. 1881–1893, May 2020.

[8] I. Andrussow, H. Sun, K. J. Kuchenbecker, and G. Martius, "Minsight: A Fingertip-Sized Vision-Based Tactile Sensor for Robotic Manipulation," *Advanced Intelligent Systems*, vol. 5, no. 8, p. 2300042, 2023.

[9] C. Lin, Z. Lin, S. Wang, and H. Xu, "DTact: A Vision-Based Tactile Sensor that Measures High-Resolution 3D Geometry Directly from Darkness," Sept. 2022. arXiv:2209.13916 [cs].

[10] V. Kakani, X. Cui, M. Ma, and H. Kim, "Vision-Based Tactile Sensor Mechanism for the Estimation of Contact Position and Force Distribution Using Deep Learning," *Sensors*, vol. 21, p. 1920, Jan. 2021. Publisher: Multidisciplinary Digital Publishing Institute.

[11] Y. Zhang, Z. Kan, Y. A. Tse, Y. Yang, and M. Y. Wang, "FingerVision Tactile Sensor Design and Slip Detection Using Convolutional LSTM Network," Oct. 2018. arXiv:1810.02653 [cs].

[12] J. Zhao, N. Kuppuswamy, S. Feng, B. Burchfiel, and E. Adelson, "PolyTouch: A Robust Multi-Modal Tactile Sensor for Contact-rich Manipulation Using Tactile-Diffusion Policies," Apr. 2025. arXiv:2504.19341 [cs].

[13] S. Wang, Y. She, B. Romero, and E. Adelson, "GelSight Wedge: Measuring High-Resolution 3D Contact Geometry with a Compact Robot Finger," in *2021 IEEE International Conference on Robotics and Automation (ICRA)*, pp. 6468–6475, May 2021. ISSN: 2577-087X.

[14] P. Potdar, D. Hardman, E. Almanzor, and F. Iida, "High-Speed Tactile Braille Reading via Biomimetic Sliding Interactions," *IEEE Robotics and Automation Letters*, vol. 9, pp. 2614–2621, Mar. 2024.

[15] P. Rayamane, Z. Ji, and M. Packianather, "Design and development of a robust vision-based tactile sensor," in *2022 IEEE/ASME International Conference on Advanced Intelligent Mechatronics (AIM)*, pp. 1417–1423, July 2022. ISSN: 2159-6255.

[16] A. Yamaguchi and C. G. Atkeson, "Combining finger vision and optical tactile sensing: Reducing and handling errors while cutting vegetables," in *2016 IEEE-RAS 16th International Conference on Humanoid Robots (Humanoids)*, (Cancun, Mexico), pp. 1045–1051, IEEE, Nov. 2016.

[17] T. Liu and B. Ward-Cherrier, "The TIP Benchmark: A Tactile Image-Based Psychophysics-Inspired Benchmark for Artificial Tactile Sensors," in *Haptics: Understanding Touch; Technology and Systems; Applications and Interaction* (H. Kajimoto, P. Lopes, C. Pacchierotti, C. Basdogan, M. Gori, B. Lemaire-Semail, and M. Marchal, eds.), (Cham), pp. 94–106, Springer Nature Switzerland, 2025.

[18] C. Higuera, A. Sharma, C. K. Bodduluri, T. Fan, P. Lancaster, M. Kalakrishnan, M. Kaess, B. Boots, M. Lambeta, T. Wu, and M. Mukadam, "Sparsh: Self-supervised touch representations for vision-based tactile sensing," Oct. 2024. arXiv:2410.24090 [cs].

[19] T. Schneider, G. Duret, C. d. Farias, R. Calandra, L. Chen, and J. Peters, "Tactile MNIST: Benchmarking Active Tactile Perception," June 2025. arXiv:2506.06361 [cs].

[20] K. O. Johnson and J. R. Phillips, "Tactile spatial resolution. I. Two-point discrimination, gap detection, grating resolution, and letter recognition," *Journal of Neurophysiology*, vol. 46, pp. 1177–1192, Dec. 1981. Publisher: American Physiological Society.

[21] R. W. Van Boven and K. O. Johnson, "The limit of tactile spatial resolution in humans," *Neurology*, vol. 44, pp. 2361–2361, Dec. 1994. Publisher: Wolters Kluwer.

[22] J. C. Craig, "Grating orientation as a measure of tactile spatial acuity," *Somatosensory & Motor Research*, vol. 16, pp. 197–206, Jan. 1999. Publisher: Taylor & Francis _eprint: https://doi.org/10.1080/08990229970456.

[23] B. Rajakumar and S. K. M. Varadhan, "Evidence to support the mechanical advantage hypothesis of grasping at low force levels," *Scientific Reports*, vol. 12, p. 20834, Dec. 2022. Publisher: Nature Publishing Group.

[24] L. Birglen and T. Schlicht, "A statistical review of industrial robotic grippers," *Robotics and Computer-Integrated Manufacturing*, vol. 49, pp. 88–97, Feb. 2018.